

Citation for published version:

Mengyao Leng, Shinan Chang, Yongsheng Lian, and Hongwei Wu, "Experimental Study of the Dynamics of Water Film on an Aluminum Substrate under Wind Shear", 9th AIAA Atmospheric and Space Environments Conference, *AIAA AVIATION Forum*, (AIAA 2017-3931).

DOI:

<https://doi.org/10.2514/6.2017-3931>

Document Version:

This is the Accepted Manuscript version.

The version in the University of Hertfordshire Research Archive may differ from the final published version.

Copyright and Reuse:

Content in the UH Research Archive is made available for personal research, educational, and non-commercial purposes only. Unless otherwise stated, all content is protected by copyright, and in the absence of an open license, permissions for further re-use should be sought from the publisher, the author, or other copyright holder.

Enquiries

If you believe this document infringes copyright, please contact Research & Scholarly Communications at rsc@herts.ac.uk

Experimental Study of the Dynamics of Water Film on an Aluminum Substrate under Wind Shear

Mengyao Leng¹ and Shinan Chang²

School of Aeronautic Science and Engineering, Beihang University, Beijing 100191

Yongsheng Lian³

Department of Mechanical Engineering, University of Louisville, Louisville, KY 40292

and

Hongwei Wu⁴

School of Engineering and Technology, University of Hertfordshire, Hatfield, AL10 9AB

Aircraft icing poses a serious threat to flight safety. Unfrozen parts of impinging water on the surface of the aircraft will run back under the effect of high-speed airflow, altering liquid distribution and heat transfer characteristics. In this paper we conducted a series of experiments over a wide range of wind speed ($U_a = 17.8\sim 52.2$ m/s), film Reynolds number ($Re_f = 26\sim 128$) and inclined angle ($\alpha = 0^\circ, \pm 30^\circ, \pm 45^\circ$) to investigate the dynamics of thin water film on an Aluminum substrate. The superficial morphology of the water film were investigated by high-speed camera, and the instantaneous film thicknesses were measured by a laser focus displacement meter based on a confocal chromatic technique. The interface between the gas and liquid phases consisted of underlying thin film and multiple scaled fluctuations. The measured time-averaged film thickness data agrees with previous model predictions. Based on the experimental results, a relationship between the film thickness and the wind speed, film Reynolds number, inclined angle was proposed. A new correlation to calculate the interfacial shear stress and superficial roughness on the wavy surface is also suggested.

Nomenclature

α	=	inclined angle
δ	=	measured thickness signal
θ	=	contact angle
μ	=	dynamic viscosity
ν	=	momentum viscosity
ρ	=	density
τ	=	shear stress
f	=	interfacial shear factor
g	=	gravitational acceleration magnitude
h	=	local film thickness
Q	=	flow rate
Re_f	=	film Reynolds number
RMS	=	root mean square
U_a	=	wind speed

¹ Graduate Student, School of Aeronautic Science and Engineering.

² Professor, School of Aeronautic Science and Engineering, Email: sn_chang@buaa.edu.cn

³ Associate Professor, Department of Mechanical Engineering, Email: yongsheng.lian@louisville.edu, AIAA Senior Member.

⁴ Senior Lecturer, School of Engineering and Technology, Email: h.wu6@herts.ac.uk.

I. Introduction

AIRCRAFT icing usually occurs when super-cooled droplets from clouds impact an aircraft surface, causing a number of degradation problems and even serious threat to flight safety [1, 2]. Droplets may freeze directly after impingement at lower temperature, building up fluffy rime ice, or partially freeze when latent heat cannot be rapidly released into the ambient air in the cases of glaze ice or when the anti-icing system is working. The unfrozen part will redistribute the surface water and affect the heat transfer rate in the ice accretion process, subsequently forming uncontrolled ice beyond the ice protected area. The uncontrolled ice can severely change the aerodynamic shape and cause performance degradations [3]. On the interface between the air and liquid water, the superficial disturbances introduces additional surface roughness [4], resulting in disturbed boundary layer flow and instabilities in the ice grow-up process. For the above reasons, the presence of the liquid water on the aerodynamic surface not only increases the danger of ice accretion, but also adds complexity to icing/anti-icing predictions.

Many researchers have proposed their theoretical and computational models for the transport behavior of unfrozen water to improve the prediction accuracy of glaze ice. The Messinger model [5] was the first trial to consider liquid water in predicting ice accretion, and has been widely applied to numerical simulations. The model calculated the frozen ratio of the surface water through heat and mass conservation, and assumed that the unfrozen part completely moved downstream, regardless of the transport behavior of the surface water. However, the high speed videos taken in wind tunnels [6, 7] indicated that the surface water existed in the form of beads, films or rivulets as a consequence of the presence of water remaining stationary on the surface. At first, the impinging droplets form beads on the surface, and then their water content is regularly removed by wind or gravity. If more water is present on the surface, the beads will coalesce into water film. The rivulets appear by the runback of deformed beads, or the breakoff of film beyond the impingement limit[8].

Numerous improvements have been proposed and examined from a computational and analytical viewpoint [9, 10]. However, these models assumed undisturbed boundary layer and uniform shear stress, which introduced various limitations on the applicability of the predictions. Myers [11] proposed a model for the water film with the consideration of ambient pressure, surface tension, gravity and shear stress. Myers' model has been applied to glaze icing, runback ice ridge and anti-icing simulations [12-15]. Among the several factors, shear stress between air and liquid was found to be a key factor in the calculation of local film thickness. However, it is hard to evaluate this due to the lack of measured data. In computational fluid dynamics (CFD) simulations [12, 14, 15], the most common substitute was the wall friction stress in the boundary layer without liquid water, which was evaluated based on the control volume analysis of the layer near the body. To consider the fluctuations between gas and liquid phases would strengthen the shear, Du et al. [16] and Karev et al. [17] applied the correlation from the experimental results of the stratified flow in their computations. In regard to the surface roughness, the interval and amplitude of the interfacial waves were usually used. For example, Ueno and Farzaneh [18] separated the interfacial fluctuations from average film thickness, and solved the wavelength and amplification factor on the basis of stability analysis theory. Recent papers by Rothmyers [19, 20] included a simulation on the full interaction of the air-water-ice field with surface waves and ice roughness. It was showed that the local instantaneous thickness of the wavy liquid film had an important effect on the heat transfer and icing accretion process.

To reveal the statistical characteristics of the water transport behavior, the experimental investigations were carried out to study water dynamics at different water states. For the bead state, White [21] used a wind tunnel that provides a turbulent accelerated flow similar to flows near an unswept wing's leading edge. Results showed that the droplet runback could be correlated by a Weber-number runback threshold. The experimental investigations on the droplet shedding were conducted within a large range of wind speed and various surface wettabilities [22, 23]. The dynamics of rivulets were also investigated under effects of the air shear and surface wettability in a wind tunnel [24]. McAlister [25] reported a study on the wind-driven breakoff of rivulets on a horizontal plate subject to different normal gravitational state. Muzik et al. [26] described the properties of the water film on the airfoil and its breakup into droplets behind the profile. These experiments attributed to improving the mechanism the surface water beads and rivulets. For the continuous films, the thickness of a horizontal film flow on a wide plane was measured in a rectangular duct and investigated the spectral differences between the 2D and 3D wavy stratified flow patterns [27]. The interfacial wavy structure of a gas-sheared liquid film was observed, and the droplet entrainment mechanism was investigated [28]. Zhang et al. [29] measured the water flow over an airfoil by using a digital image projection technique under impinging aerosol droplet conditions (10~25m/s). Liu et al. [30] quantified the transient behavior of the surface water transport process and clearly represented the relationship between the film thickness and the wind speed by using an empirical scaling law in low-speed situations. The experiment studies showed that the thickness of the film was at the micro scale and accompanied with high-frequency fluctuations. The survey of the literature suggests a need for more experimental data on the liquid film under strong air shear.

There are several characteristics of shear-driven water film, such as micro-scale thickness, complex interfacial waves, high reflective surface, fast variation in time space and easiness of disturbance, which make the measurement of thickness complicated. Although with so many challenges, extensive research has been done on liquid film problems using various techniques, such as optical measurement method [27, 29], planar laser-induced fluorescence imaging [28], laser focus displacement meter [31], and capacitance probe [32]. Although many experimental and theoretical studies were carried out to investigate the water film flowing, most of them considered the gravity driven films or the two-phase flow in a vertical or horizontal tube. For the shear-driven film on a large plate, there are few previous studies reported. The objective of this study is to characterize the instantaneous thickness of the surface water film driven by high-speed airflow in order to elucidate the detailed processes pertinent to aircraft icing phenomenon and anti-icing systems. Experiments were conducted in order to investigate the flow behavior of water film subjected to different shear and gravitation conditions. The measured film thickness data were then formulated for the evolution of water film flows and superficial roughness.

II. Experiment Setup

Experiments were conducted in the open-loop ‘liquid film’ wind tunnel of the Anti-icing/de-icing research laboratory in Beihang University, China, as shown in Figure 1. The duct body of the wind tunnel, composed of the station section, contraction section, test section and diffuser section, is mounted on a support structure made by stainless steel and aluminum profile, which provides the possibility to change the inclination angle of the test section. The main part is a horizontal aluminum plate that measures 420*130 mm², of which the surface was polished to the roughness of $R_a < 0.2\mu\text{m}$. During the experiments, the test plate is flush-mounted to the bottom wall of the test section. The remaining three sides are made by flat acrylic glass, which allow optical access to the test section. The top wall is 50 mm away from the bottom. Airflow through the bottom and top walls is generated by a centrifugal blower. A honeycomb and two layers of gauzes are placed in the upstream duct of the contraction and test sections to help make the exit flow uniform. The maximum velocity at the test section exit planes is about 55 m/s.

The working fluid, distilled water, is driven by a submersible pump and passes through a supplement vessel before entering the test section at a distance of 55 mm from the inlet of test section. The water flow-rate was measured by a pre-calibrated rotameter with an accuracy of 5%. Before entering the test section, the distilled water was first elevated into a supplement vessel made of Plexiglas, which is ideal for sealing due to its hydrophobicity. The water then slowly entered the test section through a 100 mm length groove with a rounded edge at downstream side, and flowed forward along the aluminum surface driven by the airflow. At the end of the test plane, liquid is collected in a trap through a slot in the bottom of the substrate, which is filled with an absorbent sponge material to capture the water and prevent suction of the air. As an addition, an interception net is mounted at the end of the diffuser section to reduce the trouble caused by entrained droplets.

The superficial characteristics were recorded by a high speed camera (Photron Fastcam mini UX100) and the film thickness was measured using a laser focus displacement meter (ACR-HNDS100 produced by Schmitt Industries, Inc.) based on a chromatic aberrations technique. The measurement point was located at the longitudinal centerline of

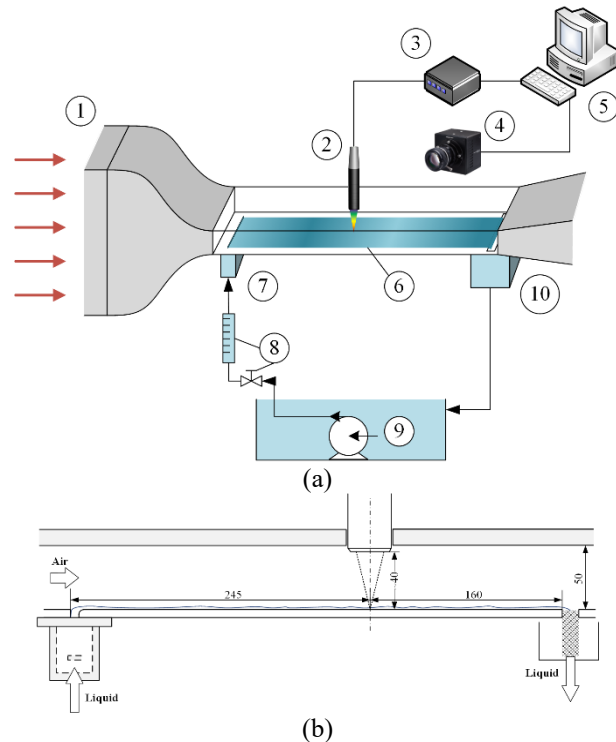


Figure 1. (a) Sketch of the rivulet wind tunnel, (b) Schematic of the test section. ① straightened airflow, ② confocal pen, ③ controller, ④ high speed camera, ⑤ computer, ⑥ test section with wind-driven film flowing on the substrate, ⑦ water reservoir, ⑧ rotameter and needle valve, ⑨ storage tank with a submersible pump, ⑩ collection vessel.

the test plane and 245 mm downstream from the outlet of the water feeding reservoir, as shown in Figure 1(b). The sensor consists of a control unit and a measure head (optical pen), with a laser spot diameter of 34 μm , and focal point distance of 37.2~45.2 mm. The system has 6-1/2 digit accuracy with stability and noise rejection. The linearity of the sensor output was calibrated as below 0.27%. During the measurement, a time record of 20,000 data points was collected for each run, and the time interval was 0.0005s.

In order to characterize the turbulent boundary layer in the test section, Particle Image Velocity (PIV) technology was performed to give boundary-layer velocity profiles in the absence of water film flows. Figure 2 shows the time-average velocity profiles in the cases of different wind speeds. In the dimensionless expressions, the velocity profile of the boundary layer airflows were found to follow the law of $U/U_a=(z/\Delta)^{1/7}$, that means a typical turbulent boundary layer flow. U is the velocity magnitude at the point which locates z from the Aluminum substrate, and Δ is the boundary layer thickness.

The experimental parameters are listed in Table 1. All the tests were carried out at room temperature in stable state, that is, the width of the film did not change before it reached the measurement location. The wind speed varied between 17.8 m/s and 52.2 m/s, and the film Reynolds number, Re_f varied within the range of 26 ~ 138. Re_f is defined as $Q/w\nu_w$, where Q is the volumetric liquid flow rate per second, ν_w is the kinematic viscosity of water, and the width of the film, w , was measured from the pictures taken by camera. For the wind speed and Reynolds number in the current range, a continuous film was expected on the aluminum substrate. The experiment procedure was the following. The surface of the aluminum was polished and cleaned with 95% alcohol before each test. Then the distilled water was pumped into the supplement vessel where it was held until the wind speed reached steady. As a stable shear-driven liquid film was formed on the test surface, the sensor started to measure the film thickness. Each test was repeated three times.

Table 1. Parameters of film flow experiment.

Parameter	Symbol	Value	Unit
Air velocity	U_a	17.8 ~ 52.2	m/s
Water flow rate	Q	200 ~ 1000	ml/min
Inclined angle	α	0, ± 30 , ± 45	$^\circ$
Substrate material	/	Aluminum	
Contact angle	θ_e	70	$^\circ$

III. Results and Discussions

A. Instantaneous Film Thickness

Typical recorded results of the film thickness by the laser focus displacement meter are shown in Figures 3 ~ 5, along with the corresponding images from the high-speed camera. The films consisted of the underlying water layer occupied by multiple waves. The instability on the films occurred when the viscous dissipation was insufficient to balance the energy transfer to a corresponding neutral wave[33]. Although the variations of the instantaneous film thickness with the wind speed or film flow rate were continuous and smooth, the film flows could be basically separated into two different flow regions: the “3D region” and the “roll-wave region”. In the 3D region, only three-dimensional ripples appeared above the underlying water film. The ripples were characterized by small magnitude and high-frequency and moved slowly along with the underlying water layer. When the flow-in mass increased, the inertia of surficial water dominated the viscous force. The underlying viscous layer cannot transport the total amount of liquid, and rolling waves formed with higher velocity and larger magnitude above the underlying layer and the ripples. Rolling waves make the analysis of film thickness more complicated, since chasing and coalescence happen in this region. Furthermore, the droplet entrainment phenomenon would be observed when the wind speed and flow

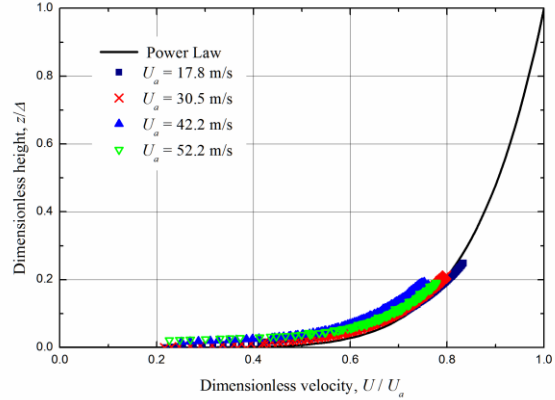


Figure 2. Averaged PIV measurement results of the boundary layer airflow over the test substrate without the surface water film. Measured results with $U_a = 17.8$ m/s, 30.5 m/s, 42.2 m/s, 52.2 m/s, respectively.

rate are both high. Detailed descriptions about the variation of film thickness with the flow rate, wind speed and inclined angles are presented in the following.

Figure 3 shows the variation of large waves with the film Reynolds number Re_f . The left figures show the time series of the measured film thickness, while the right images were taken by the high-speed camera simultaneously. In the images, the crests of interfacial waves are represented by the brighter locations and the flow direction is from left to right. The camera obtained instantaneous distributions of film thickness at 1280×1024 points, which gave a spatial resolution of 0.04 mm. The three-dimensional wavy structure can be clearly captured, including the width and length. The instantaneous thickness under the corresponding conditions are presented on the left in a duration of 10s. For smaller Reynolds numbers, such as $Re_f = 38$, the film was thinner and covered with high-frequency ripples. The ripples were orderly and steady, characterized by uniform amplitude and wave length. As the liquid flow rate increased, the ripples quickly evolved into irregular waves with large amplitudes. These waves are also called the Kelvin–Helmholtz (K–H) waves. Their inception can be associated with pressure variations in phase with the wave height [34]. These waves moved faster due to their larger amplitudes. When the rolling waves passed by, the ripples were temporally wiped at the tail part of the rolling waves and quickly appeared again. Although the movement of the large waves has a certain impact, it was observed that the thickness of the underlying layer and the ripples keep a similar shape except for the increased frequency of the large wave with increasing Re_f .

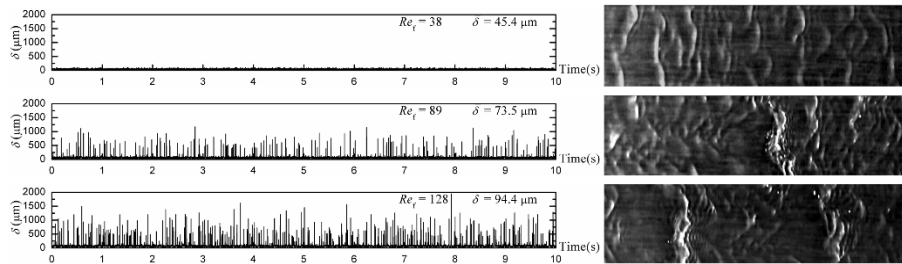


Figure 3. Instantaneous thickness of water film under different liquid flow rates. Wind speed $U_a = 30.5 \text{ m/s}$. Liquid Reynolds number, from top to bottom, $Re_f = 38, 89, 128$, respectively.

Both the ripples and large waves showed an obvious variation when the wind speed U_a varies (Figure 4). For the low wind speed cases, the underlying water layer was much thicker and had a smoother surface. The large-amplitude waves were more likely to occur at lower wind speed, and the ripples on the surface were formed by the push and squeeze from the front line of the large waves. The frequency of the ripples on the film surface reached a peak at the maximum wind speed $U_a = 52.2 \text{ m/s}$. The curvature of the waves also increased with the increasing wind speed. Compared to the effects from the water flow rate, the variations of the large waves with decreasing U_a are reflected not only in terms of the frequency but also the shape. This indicates that the wind speed is the main influence on the interfacial shape. This can be explained by Kelvin-Helmholtz instability theory [33]: when a two layer fluid has differential velocity, the interface will distort due to the momentum transfer. If only flow rate changes and the relative velocity stays the same, the distortion of interfacial shape will be similar, and only the frequency of rolling waves increases to transport the water mass.

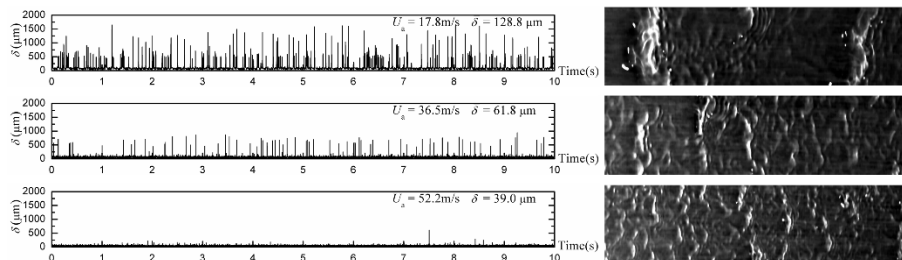


Figure 4. Instantaneous thickness of water film under different wind speeds. Liquid Reynolds number $Re_f = 89$. Wind speed, from top to bottom, $U_a = 17.8 \text{ m/s}, 36.5 \text{ m/s}, 52.2 \text{ m/s}$, respectively.

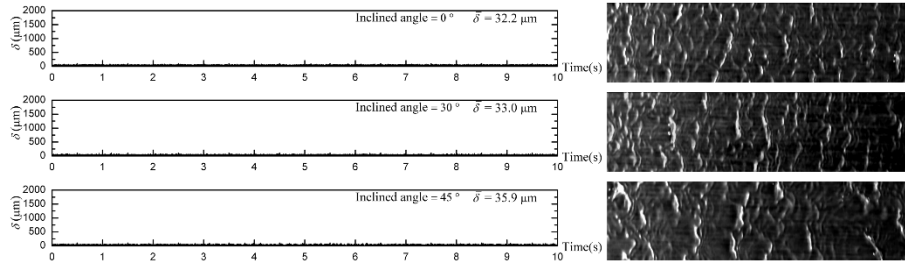


Figure 5. Instantaneous thickness of water film under different inclined angles. Liquid Reynolds number Re_f is about 51. Wind speed $U_a=52.2$ m/s. Inclined angle, from top to bottom, $\alpha = 0^\circ$, $\alpha = 30^\circ$, $\alpha = 45^\circ$, respectively.

Figure 5 shows the variation of the water films flowing on the plates of different inclined angles. In this paper, if the inclined angle was positive, it meant that the exit of the test section was higher than the inlet and the gravity had an opposite effect of the shear stress. The figure shows the comparisons between three gravitational conditions. Under the strong effect of air shear, gravity has a weak influence on interfacial shape. The average film thickness and the flow patterns were in the same section. The superficial roughness shows a slight increase with the inclined angle. For example, the roughness values for the inclined angles of 0° , 30° and 45° were $14.6 \mu\text{m}$, $14.9 \mu\text{m}$, and $16.9 \mu\text{m}$, respectively. Since the gravity introduced a backflow tendency to water, the superficial waves needed larger amplitudes to get a stronger driven force from the air stream, accompanied by longer lengths and intervals.

B. Average Film Thickness and Superficial Roughness

The time-averaged film thicknesses was calculated by $\bar{\delta} = \frac{1}{n} \sum_{i=1}^n \delta_i$, where n is the number of the collected values of the film thickness. In general, the average film thickness $\bar{\delta}$ gradually increases with decreasing wind speed or an increasing film Reynolds number, but these dependences have cross-impact. In the cases of higher wind speed, the dependences of the average film thickness on Re_f are suppressed. For instance, when $U_a = 17.8$ m/s, the average film thickness increases from $63 \mu\text{m}$ to $167 \mu\text{m}$ as the film Reynolds number varies from 26 to 128, while in the case of the maximum wind speed, the average thickness increases by $25 \mu\text{m}$ for the same range of Re_f . Similarly, for lower Re_f , the average film thickness varies slightly with the wind speed.

Given a certain liquid mass flowrate and wind speed, the local film thickness can be related to the transport ability of the surface water. To establish the relationship between the film thickness and the influence factors, a continuous steady water film driven by air shear over the surface is considered in the current work, as shown in Figure 6. Based on the lubrication theory [35], it is assumed that the changes across the film happen over a much shorter length scale than those along the film, the dominant terms may then be picked out with an appropriate

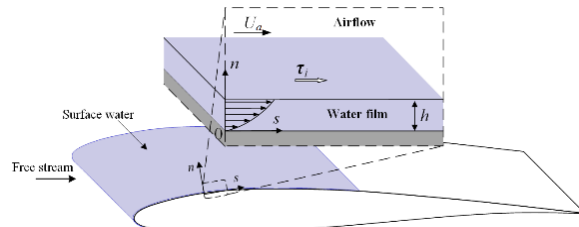


Figure 6. Schematic diagram of water film flow model

scaling. Since the ambient pressure will generally remain constant except the location near the inlet, $\frac{\partial p_a}{\partial s} = 0$. When concentrating on the film far enough away from the inlet, the terms involving derivatives of h and acting to bring the film toward its equilibrium height can be negligible [13]. A concise formula for the equilibrium height of the water film could be obtained, which is the real root of [16]

$$2\rho g \sin \alpha h^3 + 3\tau h^2 = 6\mu Q \quad (1)$$

If the air stress equals zero, then a simpler relation can be obtained as

$$h_s = \left(\frac{3\mu Q}{\rho g \sin \alpha} \right)^{1/3} \quad (2)$$

which is known as the classical model for the thickness of falling film derived by Nusselt, which has been proved practicable in a large range of inclined angles and liquid flow rates by experiments [31, 32]. On the other

hand, in the case of horizontal flow or much larger air shear, the thickness of the liquid film flow can be calculated by

$$h_s = \sqrt{\frac{2\mu Q}{\tau}} \quad (3)$$

where the viscosity of liquid μ and the flow rate Q are experimentally accessible parameters to get the film thickness. It seems that the interfacial shear stress on the water film surface, τ , becomes the key factor to determine the film thickness. It is obviously insufficient to take the skin friction force as τ , because the skin friction force refers to airflow along the surface of a smooth solid flat plate, and takes no account of the features of the water surface [17]. Since even minor surface perturbation have a considerable influence on air shear stress and also increase the interfacial friction factor, the best way to relate interfacial shear stress to airspeed and film flow rate is experimentally.

From the previous studies on interfacial friction over a wavy gas-liquid interface, the relationship between air speed and shear stress can be written as:

$$\tau = f \frac{1}{2} \rho_a U_a^2 \quad (4)$$

where f is the interfacial shear factor, U_a is the mainstream air speed. There have been several correlations for f , separately in the form of linear or power functions, depending on the experimental range of Re_f and the operation circumstances [36-38]. Through the post-processing of the data from the horizontal experiments, a correlation of the interfacial shear will be established for the prediction of the average film thickness. Then the results under the conditions with different inclined angles will be used as verification. Figure 7 presents the interfacial shear factor calculated from the equations (3) and (4) versus the film Reynolds number. The results can fit the following formula within relative error of 20%:

$$f = 0.106 Re_f^{-0.133} \quad (5)$$

Comparisons with the previous models can validate the experimental results. Based on a commonly used approximation in annular flow, referred to as the ‘triangular relationship’ between the time-averaged film thickness, the liquid flow rate and the average shear stress in film [39], it is postulated that when any two of the three variables are known, then it is possible to predict the third one. To establish the correlation, the average film thickness is non-dimensionalized by the interfacial shear stress:

$$\delta^+ = \frac{u^* \bar{\delta}}{v_L} \quad (6)$$

Table 2. Dimensionless film thickness relations and their application range

Author	Application range	Re_f	Relation
Kosky & Staub	Horizontal condense flow	13-370	$\delta^+ = 1.316 Re_f^{0.529}$
Hughmark	Upward flow	25-250	$\delta^+ = 0.874 Re_f^{2/3}$
Asali	Vertical annular flow	20-300	$\delta^+ = 0.781 Re_f^{0.6}$
Present work	Horizontal plate flow	26-128	$\delta^+ = 1.292 Re_f^{0.5289}$

where v_L is the momentum viscosity of the liquid phase, $u^* = (\tau_L / \rho_L)^{1/2}$ is the wall friction velocity defined using the shear stress τ_L inside the liquid film and the liquid density. Considering the force balance on a steady film flow, the shear stress across the film is equal to the interfacial shear stress. The values of δ^+ and dimensionless liquid rates Re_f could be obtained from the experimental data. The relationship between them is plotted in Figure 8. The present data are compared with some widely used prediction models, showing a good agreement. The relationship derived by Kosky and Staub [40] considers an annular condense film in a horizontal tube, which is closest to the present conditions and gives the best prediction for the experimental results. Hughmark’s [41] model is based on the experiments of upward annular flow. It matches the present results when $Re_f < 40$, but over-predicts the results in the range of large film Reynolds numbers, which is thought to be caused by the influence of the gravity. The Asali [42] model, which is for a downward annular film flow under gas shear stress, has the same tendency with the present results, but the dimensionless film thickness is overall smaller than that of horizontal flow.

The average thickness of the water film is the real root of the simple cubic equation (Eqn. 1). In the cases that the gravity has the opposite direction of the shear stress, the continuous film could form on the substrate only when shear stress is sufficiently strong. The minimum wind speeds needed in the cases of the specified inclined angles

were calculated from the equation before the experimental tests. Considering the stability in running the system, the tested speeds were higher than the theoretical values. So the minimum wind speed in the case of inclined angle 30° was 24.6 m/s, while in the case of 45° was 36.5 m/s. The predictions for the average film thickness using equations (1) and (4) were plotted against the film Reynolds number in Figure 9. The symbols represent the experimental measurements, while the lines represent the theoretical predictions. Agreement could be seen between the experimental results and the predictions. It shows that the shear stress dominates in the film flows and the effect of gravity is indicated in the aspect of superficial roughness.

An important characteristic of the intensity of the film fluctuations is the root-mean-square (RMS), which can be calculated using $RMS = \left[\frac{1}{n} \sum_{i=1}^n (\delta_i - \bar{\delta})^2 \right]^{1/2}$, where n is

the number of the collected values of the film thickness. The superficial roughness has a similar variation tendency to the average film thickness with the wind speed, flow rate and inclined angle. Therefore, the variations of the roughness height and the average film thickness are highly relevant, while the roughness varies more intensely. In the horizontal case, the minimum value of RMS was $7.6 \mu\text{m}$, which was about half of the minimum average film thickness. Then RMS increased strongly with increasing Re_f and decreasing U_a due to the additional large amplitude waves, and became even higher than the average film thickness in the cases of thicker films. The thinner films generally flowed in the 3D region, while the thicker films flowed in rolling wave. Due to the obviously different interfacial shape, it is reasonable to establish the correlations between the RMS and average film thickness separately for the ‘3D wave’ regime and ‘roll wave’ regime. For simplification the form, $\bar{\delta} = 40 \mu\text{m}$ is chosen as the transition point. Therefore, a piecewise linear relationship between the superficial roughness and average film thickness is employed as:

$$RMS = \begin{cases} A \times \bar{\delta} & \bar{\delta} \leq 40 \mu\text{m} \\ B \times \bar{\delta} - C & \bar{\delta} > 40 \mu\text{m} \end{cases} \quad (7)$$

Table 3. Constant values in RMS correlation for different cases

Cases	Constant A	Constant B	Constant C
$\alpha = -45^\circ$	0.6	0.97	12.6
$\alpha = -30^\circ$	0.58	1.1	11.4
$\alpha = 0^\circ$	0.5	1.6	48.0
$\alpha = 30^\circ$	0.55	1.8	49.2
$\alpha = 45^\circ$	0.57	1.4	30.9

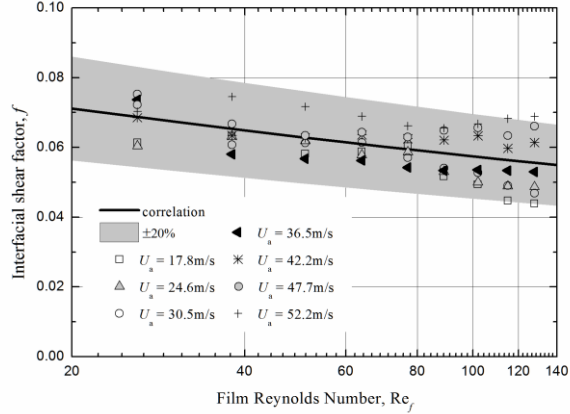


Figure 7. The variation of air shear stress with the film Reynolds number and the air speed. The black line is the best correlation curve proposed by this paper.

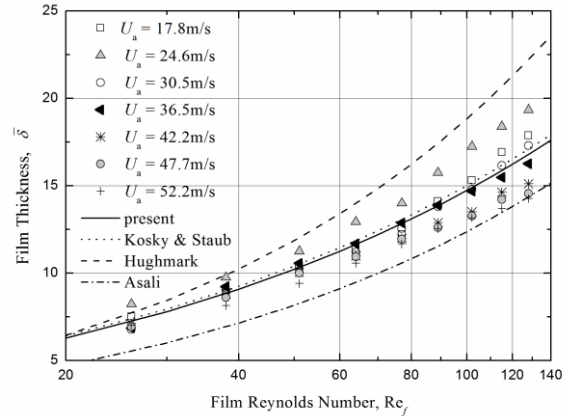
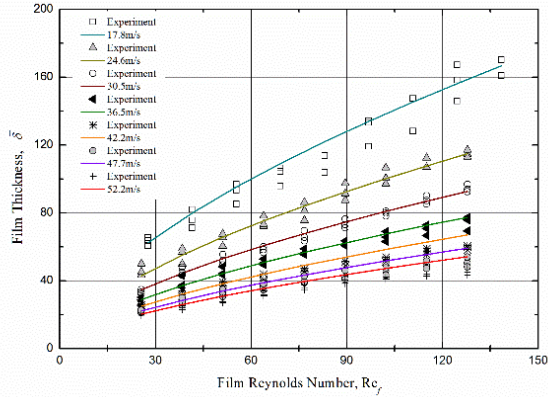
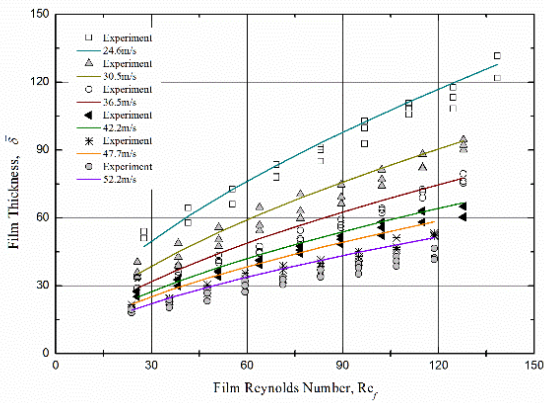


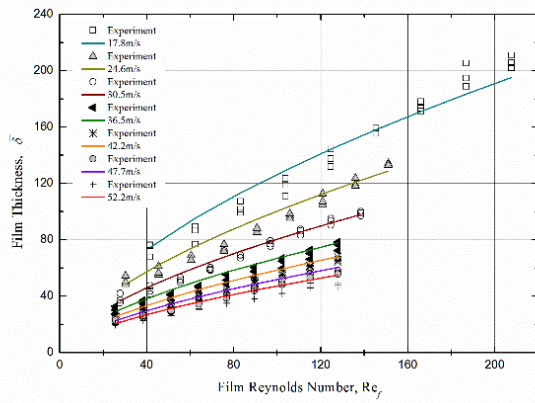
Figure 8. Comparison of measured dimensionless film thickness with correlations.



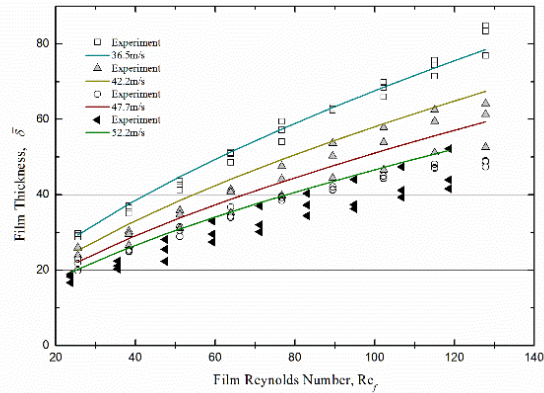
(a)



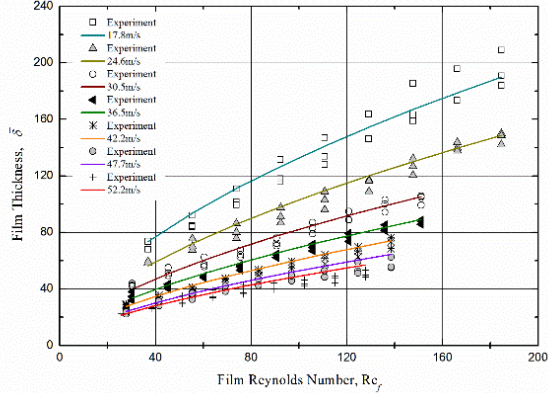
(b)



(c)



(d)



(e)

Figure 9. Statistical results of the average film thickness vs film Reynolds number under the inclined angle of (a) 0° (b) 30° (c) -30° (d) 45° (e) -45°. Different color lines are different air speed.

The constants in equation (7) were calculated from the least squares method and shown in Table 3. It can be seen that the roughness increased with the inclined angle. When the gravity has the same direction of the air shear, the inclined angle is negative, and the RMS will reduce if given the same average film thickness. On the other hand, if the gravity has the opposite direction, the roughness will increase. There is an unexpected point in the case that the inclined angle equals 45°, which should present the highest values. Since the experiments of 45° were only conducted for thinner films, the superficial roughness was in a relatively smaller range.

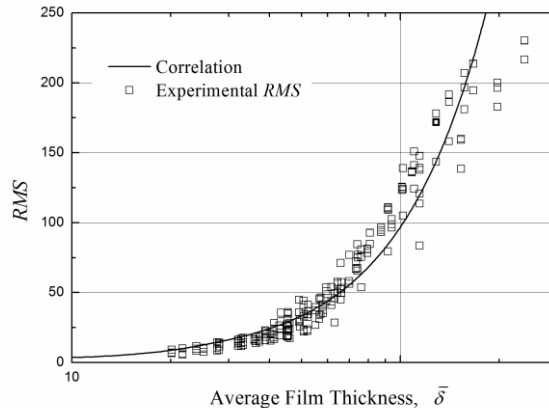


Figure 10. Variations of RMS of film thickness fluctuations with average film thickness.

IV. Conclusions

For the purpose of elucidating the detailed processes pertinent to aircraft icing and anti-icing modeling, this study conducted the measurements of the sheared water flow film on an aluminum substrate. The experiments involved three parameters: wind speed, film Reynolds number and inclination angle. Qualitative observation of the superficial structure was obtained, and quantitative descriptions on the average film thickness and superficial roughness were also well presented. The results showed that the film thickness increased with the increasing liquid flow rate and decreasing wind speed, and the gravitation condition introduced weakly additive effects. A new correlation for calculating the interfacial shear stress between two phases was suggested. The present time-average film thickness data were compared with the theoretical results in a dimensionless form showing good agreement. The correlation could be used for the prediction of the local film thickness on aircraft surface, and provide a better understanding of the characteristics of the water film flowing during the aircraft icing process.

Acknowledgments

This work was financially supported by National Basic Research Program of China under Grants No. 2015CB755803.

References

- ¹Parent, Olivier, and Adrian Ilinca. "Anti-Icing and De-Icing Techniques for Wind Turbines: Critical Review." *Cold Regions Science and Technology*, Vol. 65, no. 1, pp.88-96, 2011.
- ²Gent, R. W., N. P. Dart, and J. T. Cansdale. "Aircraft Icing." *Philosophical Transactions of the Royal Society A: Mathematical, Physical and Engineering Sciences*, Vol. 358, no. 1776, pp.2873-911, 2000.
- ³Whalen, Edward A., Andy P. Brocroun, and Michael B. Bragg. "Aerodynamics of Scaled Runback Ice Accretions." *JOURNAL OF AIRCRAFT*, Vol. 45, no. 2, pp.591-603, 2008.
- ⁴Streitz, Jeffrey T., and Robert Etema. "Observations From an Aufeis Windtunnel." *Cold Regions Science and Technology*, Vol. 34, no. 2, pp.85-96, 2002.
- ⁵Messinger, Bernard L. "Equilibrium Temperature of an Unheated Icing Surface as a Function of Air Speed." *Journal of the Aeronautical Sciences*, Vol. 20, no. 1, pp.29-42, 1953.
- ⁶Hansman, R. John, and Stephen R. Turnock. "Investigation of Surface Water Behavior During Glaze Ice Accretion." *Journal of Aircraft*, Vol. 26, no. 2, pp.140-47, 1989.
- ⁷Hansman, R. John, Keiko Yamaguchi, Brian Berkowitz, and Mark Potapczuk. "Modeling of Surface Roughness Effects On Glaze Ice Accretion." *Journal of thermophysics and heat transfer*, Vol. 5, no. 1, pp.54-60, 1991.
- ⁸Alekseyenko, S., M. Sinapius, M. Schulz, and O. Prykhodko. "Interaction of Supercooled Large Droplets with Aerodynamic Profile." 2015.
- ⁹Al-Khali, Kamel M., Jr. Theo G. Keith, and Kenneth J. De Witt. "Development of an Improved Model for Runback Water On Aircraft Surfaces." *JOURNAL OF AIRCRAFT*, Vol. 31, no. 02, pp.271-78, 1994.
- ¹⁰Fortin, Guy, Jean Louis Laforte, and Adrian Ilinca. "Heat and Mass Transfer During Ice Accretion On Aircraft Wings with an Improved Roughness Model." *International Journal of Thermal Sciences*, Vol. 45, no. 6, pp.595-600, 2006.
- ¹¹Myers, Tim G., and Chris P. Thompson. "Modeling the Flow of Water On Aircraft in Icing Conditions." *AIAA journal*, Vol. 36, no. 6, pp.1010-13, 1998.
- ¹²Harireche, Ouahid, Patrick Verdin, Chris P. Thompson, and David W. Hammond. "Explicit Finite Volume Modeling of Aircraft Anti-Icing and De-Icing." *Journal of Aircraft*, Vol. 45, no. 6, pp.1924-36, 2008.

- ¹³ Yanxia, Du, Gui Yewei, Xiao Chunhua, and Yi Xian. "Investigation On Heat Transfer Characteristics of Aircraft Icing Including Runback Water." *International Journal of Heat and Mass Transfer*, Vol. 53, no. 19-20, pp.3702-07, 2010.
- ¹⁴ Myers, T. G. "Extension to the Messinger Model for Aircraft Icing." *AIAA JOURNAL*, Vol. 39, no. 2, pp.211-18, 2001.
- ¹⁵ Cao, Y., J. Huang, and J. Yin. "Numerical Simulation of Three-Dimensional Ice Accretion On an Aircraft Wing." *International Journal of Heat & Mass Transfer*, 2016.
- ¹⁶ Karev, A. R., M. Farzaneh, and E. P. Lozowski. "Character and Stability of a Wind-Driven Supercooled Water Film On an Icing Surface—I. Laminar Heat Transfer." *International Journal of Thermal Sciences*, Vol. 42, no. 5, pp.481-98, 2003.
- ¹⁷ Ueno, Kazuto, and Masoud Farzaneh. "Linear Stability Analysis of Ice Growth Under Supercooled Water Film Driven by a Laminar Airflow." *Physics of Fluids*, Vol. 23, no. 4, pp.42103, 2011.
- ¹⁸ Rothmayer, Alric P., and Hui Hu. "Solutions for Two-Dimensional Instabilities of Ice Surfaces Uniformly Wetted by Thin Films." In *AIAA atmospheric and space environments conference*, 17. New Orleans, LA(US), 2012.
- ¹⁹ Wang, G., and A. P. Rothmayer. "Thin Water Films Driven by Air Shear Stress through Roughness." *Computers & Fluids*, Vol. 38, no. 2, pp.235-46, 2009.
- ²⁰ White, Edward B., and Jason A. Schmucker. "A Runback Criterion for Water Drops in a Turbulent Accelerated Boundary Layer." *Journal of Fluids Engineering*, Vol. 130, no. 6, pp.61301-02, 2008.
- ²¹ Moghtadernejad, Sara, Mehdi Jadidi, Moussa Tembely, Nabil Esmail, and Ali Dolatabadi. "Concurrent Droplet Coalescence and Solidification On Surfaces with Various Wettabilities." *Journal of Fluids Engineering*, Vol. 137, no. 7, pp.71301-02, 2015.
- ²² Milne, A. J. B., and A. Amirfazli. "Drop Shedding by Shear Flow for Hydrophilic to Superhydrophobic Surfaces†." *Langmuir*, Vol. 25, no. 24, pp.14155-64, 2009.
- ²³ Moghtadernejad, Sara, Mehdi Jadidi, Ali Dolatabadi, and Nabil Esmail. "Sph Simulation of Rivulet Dynamics On Surfaces with Various Wettabilities." *SAE International Journal of Aerospace*, Vol. 8, no. 1, pp.160-73, 2015.
- ²⁴ McAlister, G., R. Ettema, and J. S. Marshall. "Wind-Driven Rivulet Breakoff and Droplet Flows in Microgravity and Terrestrial-Gravity Conditions." *Journal of Fluids Engineering*, Vol. 127, no. 2, pp.257-66, 2005.
- ²⁵ Muzik, Tomas, Pavel Safarik, and Antonín Tucek. "Analysis of the Water Film Behavior and its Breakup On Profile Using Experimental and Numerical Methods." *Journal of Thermal Science*, Vol. 23, no. 4, pp.325-31, 2014.
- ²⁶ Touron, François, Larbi Labraga, Laurent Keirsbulck, and Hervé Bratec. "Measurements of Liquid Film Thickness of a Wide Horizontal Co-Current Stratified Air-Water Flow." *Thermal Science*, no. 00, pp.212, 2012.
- ²⁷ Cherdantsev, Andrey V., David B. Hann, and Barry J. Azzopardi. "Study of Gas-Sheared Liquid Film in Horizontal Rectangular Duct Using High-Speed LIF Technique: Three-Dimensional Wavy Structure and its Relation to Liquid Entrainment." *International Journal of Multiphase Flow*, Vol. 67, pp.52-64, 2014.
- ²⁸ Zhang, Kai, Tian Wei, and Hui Hu. "An Experimental Investigation On the Surface Water Transport Process Over an Airfoil by Using a Digital Image Projection Technique." *Experiments in Fluids*, Vol. 56, no. 9, 2015.
- ²⁹ Liu, Yang, Wen-Li Chen, Leonard J. Bond, and Hui Hu. "An Experimental Study On the Characteristics of Wind-Driven Surface Water Film Flows by Using a Multi-Transducer Ultrasonic Pulse-Echo Technique." *Physics of Fluids*, Vol. 29, no. 1, pp.12102, 2017.
- ³⁰ Zhou, D. W., T. Gambaryan-Roisman, and P. Stephan. "Measurement of Water Falling Film Thickness to Flat Plate Using Confocal Chromatic Sensing Technique." *Experimental Thermal and Fluid Science*, Vol. 33, no. 2, pp.273-83, 2009.
- ³¹ Yu, Y. Q., and X. Cheng. "Experimental Study of Water Film Flow On Large Vertical and Inclined Flat Plate." *Progress in Nuclear Energy*, Vol. 77, pp.176-86, 2014.
- ³² Cohen, Leonard S., and Thomas J. Hanratty. "Generation of Waves in the Concurrent Flow of Air and a Liquid." *AIChE Journal*, Vol. 11, no. 1, pp.138-44, 1965.
- ³³ Tzotzi, Christina, and Nikolaos Andritsos. "Interfacial Shear Stress in Wavy Stratified Gas - Liquid Flow in Horizontal Pipes." *International Journal of Multiphase Flow*, Vol. 54, pp.43-54, 2013.
- ³⁴ Wu, W. Y. *Fluid Dynamics*: Peking University Press, 2004.
- ³⁵ Miya, Masayoshi, Donald E. Woodmansee, and Thomas J. Hanratty. "A Model for Roll Waves in Gas-Liquid Flow." *Chemical Engineering Science*, Vol. 26, no. 11, pp.1915-31, 1971.
- ³⁶ Ishii, M., and M. A. Grolmes. "Inception Criteria for Droplet Entrainment in Two-Phase Concurrent Film Flow." *AIChE Journal*, Vol. 21, no. 2, pp.308-18, 1975.
- ³⁷ Cheremisinoff, Nicholas P., and E. James Davis. "Stratified Turbulent - Turbulent Gas - Liquid Flow." *AIChE journal*, Vol. 25, no. 1, pp.48-56, 1979.
- ³⁸ Zhao, Yujie, Christos N. Markides, Omar K. Matar, and Geoffrey F. Hewitt. "Disturbance Wave Development in Two-Phase Gas - Liquid Upwards Vertical Annular Flow." *International Journal of Multiphase Flow*, Vol. 55, pp.111-29, 2013.
- ³⁹ Kosky, Philip G., and Fred W. Staub. "Local Condensing Heat Transfer Coefficients in the Annular Flow Regime." *AIChE Journal*, Vol. 17, no. 5, pp.1037-43, 1971.
- ⁴⁰ Hughmark, G. A. "Film Thickness, Entrainment, and Pressure Drop in Upward Annular and Dispersed Flow." *AIChE Journal*, Vol. 19, no. 5, pp.1062-65, 1973.
- ⁴¹ Asali, J. C., T. J. Hanratty, and Paolo Andreussi. "Interfacial Drag and Film Height for Vertical Annular Flow." *AIChE Journal*, Vol. 31, no. 6, pp.895-902, 1985.